Local Demagnetization Detection in Six-Phase Permanent Magnet Synchronous Machines

Local Demagnetization Detection in Six-Phase Permanent Magnet Synchronous Machines

L. Vancini, *Member, IEEE*, M. Mengoni, *Member, IEEE*, G. Rizzoli, L. Zarri, *Senior Member, IEEE,* and A. Tani

***Abstract* – The partial demagnetization process in Surface-Mounted Permanent-Magnet Synchronous Motors (SMPMSMs) negatively affects the performance of an electric drive, reducing the rated torque and the efficiency of the machine. This paper presents a comprehensive analysis of the rotor demagnetization caused by an overcurrent event for a six-phase SMPMSM. Multiphase drives may become a key solution for safety-critical applications because they allow one to increase the intrinsic reliability of the electric systems and monitor the health state of electric motors and power converters.**

This paper proposes a diagnostic algorithm for the online detection of rotor demagnetization faults that also considers the magnetization direction of the magnets. The effects of the parallel or radial magnetization of the rotor magnets are analyzed for multiphase machines. The technique quantifies the demagnetization degree to estimate the fault severity and corrects the angular position of the encoder to ensure maximum motor performance under post-fault conditions.

Experimental tests have been carried out on two identical six-phase PMSMs differing only in the size of the rotor magnets to emulate the effect of a trailing-edge demagnetization. The experimental results confirm the effectiveness and robustness of the proposed solution.

***Index Terms* - Multiphase motor drives, permanent-magnet synchronous motor (PMSM), local demagnetization, fault detection.**

I. INTRODUCTION

Permanent-magnet synchronous machines (PMSMs) are crucial in many modern applications. PMSMs are widely used in the automotive industry due to their simple structure and high power density [1] – [3]. The same characteristics make these electric machines competitive in the emerging field of More Electric Aircraft (MEA) and Full Electric Aircraft (FEA) [4] - [7].

However, the main flaw of this technology is represented by the permanent magnets (PMs), which are safety-critical components [7]. Machines that experience a demagnetization fault may cause a loss of service continuity and require high maintenance and replacement costs.

Above the Curie temperature the thermal disorder causes the irreversible loss of the magnetic properties in permanent magnets. The Curie temperature of SmCo and NdFeB magnets is well above 300 °C, much higher than the typical internal temperatures observed in electrical machines. However, even below the Curie point, the remanence and intrinsic coercivity of PMs reduce as the temperature rises. Therefore, as the temperature increases, the material is more susceptible to local demagnetization due to the magnetic field generated by the stator current during regular operation or in the event of short circuits and overcurrent conditions. While the temperature causes a uniform demagnetization of the magnets, the overcurrent produces a partial and local demagnetization, whose position depends on the orientation of the magnetic field generated by the stator current.

Therefore, in PMSMs, the irreversible demagnetization is results from the combined effect of high-temperature operation and a strong reverse magnetic field generated by the stator currents. The problem of demagnetization induced by a stator overcurrent is even more significant in motors with ferrite magnets, which have much lower intrinsic coercivity than rare-earth magnets. Therefore, online monitoring techniques for the health state of PMs are crucial diagnostic tools in motor drives without rare-earth PMs [8]. These applications aim to replace high-energy rare-earth magnets with ferrites to reduce costs and increase the raw materials availability [9] - [11].

For these reasons, several methods for diagnosing demagnetization faults in three-phase PMSMs have been reported in the literature [12]. The most traditional approaches are based on the Current Signature Analysis (CSA) and the spectrum of the back-Electro Motive Force (back-EMF) [13] - [14]. These solutions search for the harmonic signature of the fault using mathematical tools such as the Hilbert and Wavelet transform. Partial demagnetization of the rotor magnets modifies the distribution of the magnetic field in the air gap. This allows the fault to be detected by analyzing the harmonic content of the phase current and voltage. This approach typically has a high computational cost and requires large memory buffers for online data processing.

Other recent diagnostic methods use convolutional neural networks, which have the task of recognizing failure patterns and signatures [15] - [17]. This approach is versatile because it can potentially identify many types of faults with very short response times and good reliability. The main drawback of this technology is the training of the neural network, which requires large amounts of data generated by numerical simulations or experimental results.

Finally, the most accurate and reliable methods use probes and sensors inside the electric machine. These intrusive solutions directly monitor the magnetic field in the air gap in any operating condition of the motor. Although these methods are robust, the presence of sensors must be considered during the motor design phase. The additional measuring instrument are relatively inexpensive, such as Hall effect probes [18] -

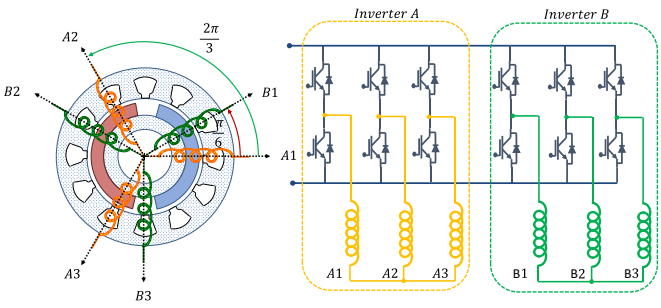

Fig. 1. Six-phase PMSM with a spatial shifting of $\pi/6$ between three-phase windings and a dual three-phase inverter.

[20] or a dedicated search coil [21]-[22]. In addition, the direct measurement of the magnetic field in the airgap ensures the detection of other faults, such as rotor eccentricity and stator winding unbalance. As a results, these methods are versatile, provide immediate results and do not require complex processing units.

Probably, the most widely used multiphase system is the six-phase machine. The stator windings of an asymmetrical six-phase motor consist of two three-phase windings shifted by 30° (electrical degrees). The increased number of stator phases results in the inherent fault tolerance that is a characteristic feature of multiphase drives. Multi-three-phase motor drives can be easily obtained by rearranging the winding of a traditional three-phase machine and using standard three-phase inverters connected to the same DC-link (Fig. 1). Therefore, they are one of the most common multiphase solutions [23] - [25].

In addition, multiphase machines are characterized by more degrees of freedom than three-phase machines. The new variables can be used to monitor the state of health of the multiphase motors. Despite the extensive literature on the numerous advantages of multiphase machines, few contributions focus on the detection of a demagnetization fault [26] - [27].

This paper presents an algorithm to detect and estimate the local demagnetization of the rotor magnets. The proposed method is based on a mathematical model of the magnetic field generated by the rotor magnets in a multiphase machine, taking into account the direction of the magnetization of the magnets (radial or parallel). The analyzed solution is quite different from those developed for three-phase motors because it fully exploits the degrees of freedom of multiphase systems to increase the robustness and reliability of the fault diagnosis. Furthermore, the analytical results show that the trailing-edge demagnetization fault leads to a non-perfect field orientation of the control system, which reduces the post-fault torque capability and efficiency of the machine. The proposed algorithm corrects the angular position to maximize the motor performance compatible with the fault effects.

Overall, the main contributions and advantages investigated in this paper are as follows:

- analytical description of the magnetic field generated by the rotor magnets in a multiphase machine taking into account the magnetization direction of the magnets (radial or parallel);
- definition of an algorithm to estimate and quantify the partial demagnetization of rotor magnets;
- angular realignment of the control system for maximum torque capability after the detection of the demagnetization fault;
- robustness against the variation of the electrical parameters of the motor;
- low computational burden and no data storage.

This paper is organized as follows. Section II illustrates the mathematical model of a six-phase PMSM. This part includes the motor equations and the analytical formulation of the magnetic field in the air gap. In Section III, the detection algorithm of the local demagnetization is described, and the block diagram of the proposed motor control system is explained in detail. Finally, in Section IV, the accuracy of the analytical model and the effectiveness of the control scheme

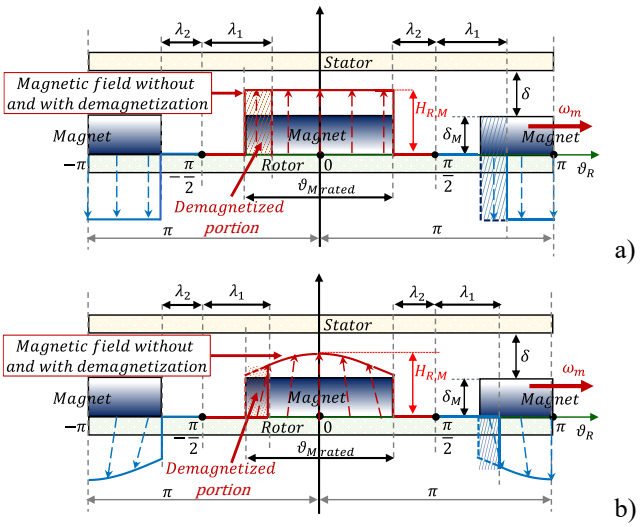

Fig. 2. Magnetic field distribution produced by magnets with radial magnetization (a) and parallel magnetization (b).

are experimentally validated using two six-phase PMSMs that differ only in the degree of demagnetization of the rotor. The tests evaluate the dynamic performance, robustness, and effectiveness of the proposed solution.

II. Mathematical Model of a Six-Phase Surface Mounted Permanent Magnet Synchronous Motor

This paper considers a six-phase PMSM with two isolated three-phase star-connected stator windings A_1, A_2, A_3 and B_1, B_2, B_3 shifted by 30° electrical degrees from each other (Fig. 1).

The mathematical model of a multiphase motor takes advantage of the Vector Space Decomposition (VSD), a linear transformation of the electromagnetic quantities that allows the machine to be represented as a set of decoupled equations in separate subspaces or planes.

A. Machine Equations

The generic expression of the ρth space vector of the stator currents i_{Ak} and i_{Bk} $(k = 1,2,3)$ is as follows:

$$\bar{\imath}_{S\rho}^{S} = \frac{2}{6}\sum_{k=1}^{3}\left(i_{Ak} + i_{Bk}\bar{\beta}^{\rho}\right)\bar{\alpha}_k^{\rho} \qquad \rho = 1,3,5. \tag{1}$$

where:

$$\bar{\alpha}_k = e^{j\frac{2\pi}{3}(k-1)}, \quad \bar{\beta} = e^{j\frac{\pi}{6}} \quad k = 1,2,3. \tag{2}$$

and the superscript "S" indicates the stationary reference frame.

It can be easily demonstrated that only three current space vectors are necessary and sufficient to satisfy the six degrees of freedom of a six-phase PMSM. Typically, the mathematical model of the motor is based on $\bar{\imath}_{S1}^{S}$ and $\bar{\imath}_{S5}^{S}$ because the common-mode current $\bar{\imath}_{S3}^{S}$ is zero due to the winding connections. The current vector $\bar{\imath}_{S1}^{S}$ is used for the motor torque and speed control, and $\bar{\imath}_{S5}^{S}$ is generally set to zero to reduce the torque ripple and stator Joule losses [28].

Linear transformation (1) can be applied to the phase voltages v_{Ak}, v_{Bk} and the fluxes $\varphi_{Ak}, \varphi_{Bk}$.

The VSD generates a set of independent equations, identified by subscript ρ ($\rho = 1,5$), which can be written in the stationary reference frame as follows:

$$\bar{v}_{S\rho}^{S} = R_S \bar{\imath}_{S\rho}^{S} + \frac{d\bar{\varphi}_{S\rho}^{S}}{dt} \quad (\rho = 1,5) \tag{3}$$

$$\bar{\varphi}_{S\rho}^{S} = L_{S\rho} \bar{\imath}_{S\rho}^{S} + \bar{\varphi}_{E\rho}^{S} \quad (\rho = 1,5) \tag{4}$$

$$T = 3\,p \sum_{\rho=1,5} \rho\, \bar{\imath}_{S\rho}^{S} \cdot \left(j\bar{\varphi}_{E\rho}^{S}\right) \tag{5}$$

where R_S and $L_{S\rho}$ are the stator resistance and inductance respectively, $\bar{\varphi}_{S\rho}^{S}$ is the stator flux linkage vector, $\bar{\varphi}_{E\rho}^{S}$ is the flux linked to the stator windings generated by the rotor magnets, $\bar{v}_{S\rho}^{S}$ is the stator voltage vector, $\bar{\imath}_{S\rho}^{S}$ is the stator current vector and p is the number of pole pairs number. Finally, the dot operator "$\cdot$" is defined as the real part of the product of the first operand and the complex conjugate of the second operand.

In a rotor field-oriented drive, the control system is implemented in the d-q reference frame, whose d-axis has the same direction as the excitation field. The current i_{S1q} is used for torque control, while i_{S1d} can reduce the stator flux due to the excitation field for field weakening operations.

Demagnetization in a permanent magnet machine can be caused by mechanical stress, overtemperature, or a demagnetizing overcurrent. The effect of temperature alone causes a uniform and reversible reduction in the magnetic properties of rotor magnets until the temperature reaches the Curie temperature. A robust diagnostic algorithm must distinguish this effect from the irreversible demagnetization caused by the magnetic field generated by an overload current.

For example, irreversible demagnetization can be caused by the stator current component i_{S1d} along the direction of the rotor magnetic field. This event may occur when the motor operates in the field weakening region, and the magnetic field generated by a high negative i_{S1d} can symmetrically demagnetize the central part of the rotor magnets in all pole pairs. The demagnetization caused by an i_{S1d} current has a significant effect on the motor performance. For this reason, it is easy to diagnose. Even the loss of magnetic properties in small portions of the central part of the magnet dramatically reduces the fundamental component of the rotor magnetic field. As a results, monitoring the torque produced or the voltage required by the motor is generally sufficient to diagnose the central demagnetization of the rotor magnets. Typically, the thickness of the magnets is designed to withstand the demagnetizing field applied during the flux weakening operation.

Conversely, an intense overload current i_{S1q} at a high temperature can cause the trailing edge demagnetization of the rotor magnets (Fig. 2). This type of fault is more common and much more challenging to diagnose due to the non-trivial effects it has on the magnetic field distribution in the air gap.

Short circuit (SC) faults can also produce the demagnetization of the rotor magnets. The SC can be caused by an insulation fault between two stator phases or within the same coil (inter-turn SC). The structure of the stator windings and the location of the fault significantly affect the characteristics of the demagnetization phenomena. If the motor is not properly designed, the simultaneous SC of all six motor phases caused by a fault in the power electronics can demagnetize the central part of the rotor magnets. However, this event is unusual in a multiphase machine because the correct sizing of the magnets prevents this type of failure, and the simultaneous fault of both inverters in a double three-phase inverter is rare. Conversely, the temporary overload of the motor with a high value of the current i_{S1q} is a common event. A significant overload may potentially cause a local demagnetization in the rotor magnets.

This article proposes a diagnostic algorithm to detect and quantify the rotor demagnetization caused by an overload current that generates a magnetic field directed along the q-axis.

The trailing-edge demagnetization can be modeled by removing a portion of the magnetic material from the edge of the rotor magnets, as shown in Fig. 2, where ϑ_R is an electrical angle used as an angular coordinate in a rotor reference frame, $\pi - \lambda_1 - \lambda_2$ $(0 \le \lambda_1 \le \pi, 0 \le \lambda_2 \le \pi - \lambda_1)$ is the magnet arc ϑ_M of the surface-mounted permanent magnets, and $\lambda_2 - \lambda_1$ is the demagnetized angular portion. Under healthy conditions, λ_1 is equal to λ_2, but partial demagnetization forces λ_1 to increase.

The physical phenomenon of demagnetization strictly depends on the direction of magnetization of the rotor magnets, which is typically radial or parallel. These two cases are discussed in the following subsection.

B. Radial Magnetization of Surface Mounted PMs

The lines in Fig. 2 (a) represent the magnetic field in the airgap generated by radially magnetized magnets. The dashed line describes the rotor magnetic field distribution under healthy conditions, whereas the solid line represents the effect of local demagnetization of a portion of a magnet. The rotor field distribution can be described mathematically as follows [28]-[29]:

$$H_R(\vartheta_R) = \begin{cases} H_{R,M} & -\frac{\pi}{2} + \lambda_1 < \vartheta_R < \frac{\pi}{2} - \lambda_2 \\ -H_{R,M} & \frac{\pi}{2} + \lambda_1 < \vartheta_R < -\frac{\pi}{2} - \lambda_2 \\ 0 & Otherwise \end{cases} \tag{6}$$

When the machine is healthy, λ_1 and λ_2 are equal.

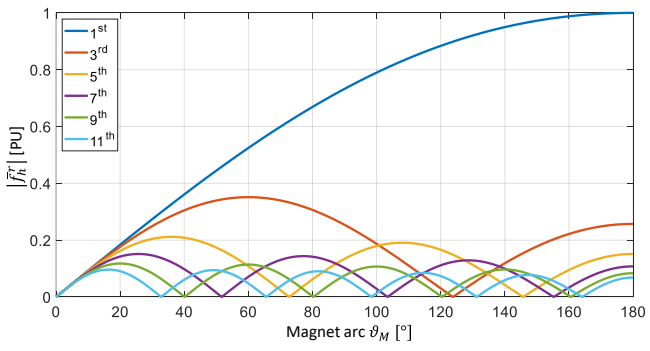

Fig. 3. Graphical description of $\left|\bar{f}_h^r\right|$ for radially magnetized magnets.

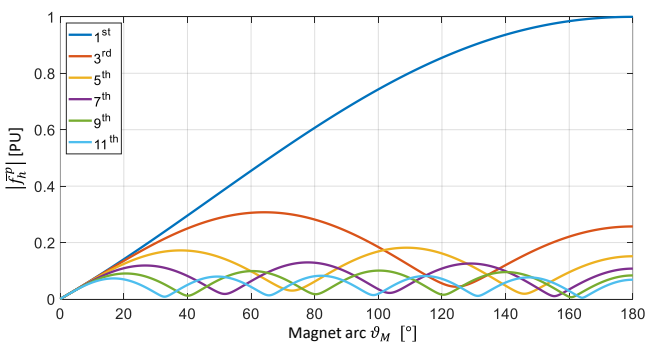

Fig. 4. Graphical description of $\left|\bar{f}_h^p\right|$ for parallelly magnetized magnets.

Conversely, after a fault, λ_1 and λ_2 take different values due to the local demagnetization of the edge of the magnets. The peak value of the rotor magnetic field is $H_{R,M}$, which can be easily calculated using Ampère's circuital law and the parameters of the magnets. The value of $H_{R,M}$ is proportional to the magnetic remanence B_R and depends on the thickness δ_M of the magnet and the distance δ between the magnets and the stator, as follows:

$$H_{R,M} = B_R \left(\frac{\delta_M}{\mu_0 \, \delta_M + \mu_d \, \delta} \right). \tag{7}$$

In (7), μ_0 is the permeability of free space and μ_d is the differential permeability of the rotor magnets.

The spatial distribution of the magnetic field in the airgap generated by the rotor can be written as a Fourier series as follows:

$$H_R(\vartheta_R) = \sum_{h=1,3,..}^{+\infty} \Re e\left[\bar{h}_{R,h} e^{-jh\vartheta_R} \right]. \tag{8}$$

The complex number $\bar{h}_{R,h}$ in (8) represents the hth spatial harmonic component of the rotor magnetic field and can be expressed as follows:

$$\bar{h}_{R,h} = \frac{2}{\pi} H_{R,M} \, \bar{f}_h(\lambda_1, \lambda_2) \tag{9}$$

where the function $\bar{f}_h(\lambda_1, \lambda_2)$ considers the type of magnetization (radial or parallel) and the demagnetization angle of the rotor magnets. In the case of radial magnetization of the magnets, $\bar{f}_h(\lambda_1, \lambda_2)$ can be expressed as follows:

$$\bar{f}_h^r(\lambda_1, \lambda_2) = \frac{1}{h}\left(e^{jh\lambda_1} + e^{-jh\lambda_2}\right)(-1)^{\frac{h-1}{2}} \tag{10}$$

while the expression of $\bar{f}_h(\lambda_1, \lambda_2)$ for parallel magnetization of the rotor is presented in the next section. In both cases, $\bar{f}_h$ is a complex function but, if the origin of the reference frame is aligned with the symmetry axis of the rotor magnetic field, the imaginary component becomes zero. The graphical representation of the magnitude of $\bar{f}_h^r$ for radial magnetization as a function of the magnet arc for a PMSM with two pole pairs is shown in Fig. 3. The peak values of $|\bar{f}_h^r|$ decrease if the harmonic order increases. The trend of the function $\bar{f}_h^r$ for the hth harmonic order is monotonic in the range $[k\pi/h \; ; (k+1)\pi/h], k \in [0,1,\dots,h-1]$.

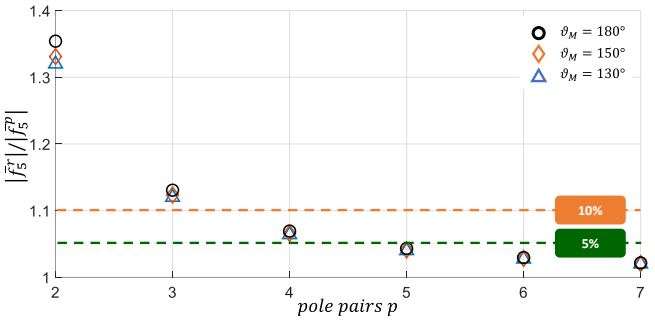

Fig. 5. Ratio between the magnitude of the 5th harmonic component of the magnetic field in the air gap in case of radial and parallel magnetization.

C. Parallel Magnetization of Surface Mounted PMs

The magnetic field distribution produced in case of parallel magnetization of PMs, represented by the dashed and the solid lines in Fig. 2 (b) for a motor with two pole pairs, can be described as follows:

$$H_R(\vartheta_R) = \begin{cases} H_{R,M} \cos\left(\dfrac{\vartheta_R}{p}\right) & -\dfrac{\pi}{2} + \lambda_1 < \vartheta_R < \dfrac{\pi}{2} - \lambda_2 \\ H_{R,M} \cos\left(\dfrac{\vartheta_R - (p-1)\pi}{p}\right) & -\pi < \vartheta_R < -\dfrac{\pi}{2} - \lambda_2 \\ H_{R,M} \cos\left(\dfrac{\vartheta_R + (p-1)\pi}{p}\right) & \dfrac{\pi}{2} + \lambda_1 < \vartheta_R < \pi \\ 0 & Otherwise \end{cases} \tag{11}$$

where $H_{R,M}$ is given by (7). The Fourier transform of (11) can be expressed by using (8) and (9), where the function $\bar{f}_h(\lambda_1, \lambda_2)$ in case of parallel magnetization is equal to:

$$\bar{f}_h^p(\lambda_1, \lambda_2) = \frac{p}{h^2 p^2 - 1}\left\{\bar{A}_2 e^{jhp\gamma_2} - \bar{A}_1 e^{-jhp\gamma_1}\right\} \tag{12}$$

and the variables $\bar{A}_1$, $\bar{A}_2$, γ_1 and γ_2 are defined as follows:

$$\begin{aligned} \bar{A}_1 &= jph\cos(\gamma_1) - \sin(\gamma_1) \\ \bar{A}_2 &= jph\cos(\gamma_2) + \sin(\gamma_2) \\ \gamma_1 &= \frac{1}{p}\left(\lambda_1 - \frac{\pi}{2}\right) \\ \gamma_2 &= \frac{1}{p}\left(\lambda_2 - \frac{\pi}{2}\right). \end{aligned} \tag{13}$$

A graphical representation of $|\bar{f}_h^p(\lambda_1, \lambda_2)|$ is provided in Fig. 4 for a healthy machine with $p = 2$.

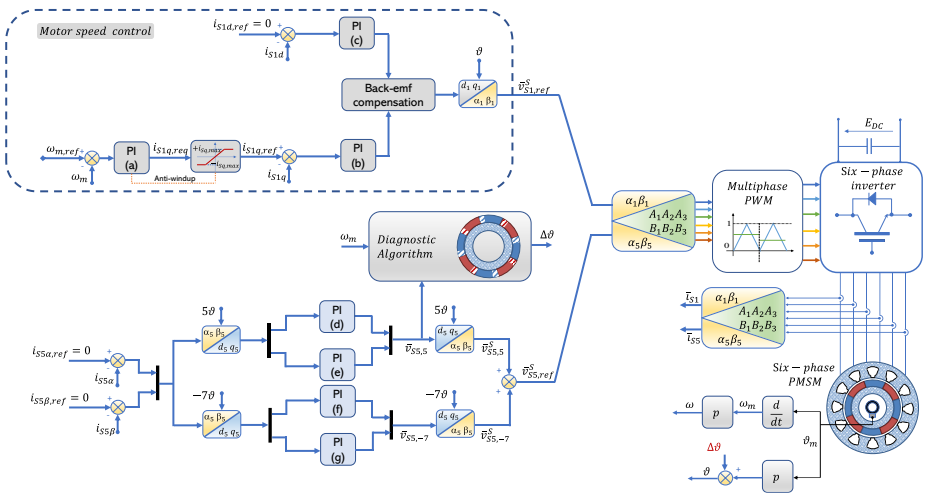

Fig. 6. Block diagram of the motor control system.

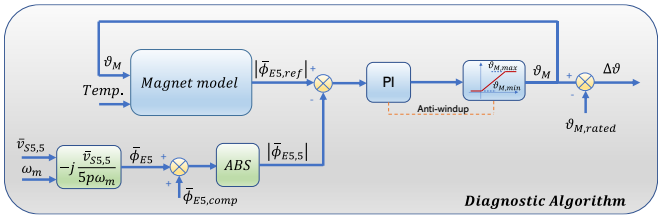

Fig. 7. Block diagram of the diagnostic algorithm.

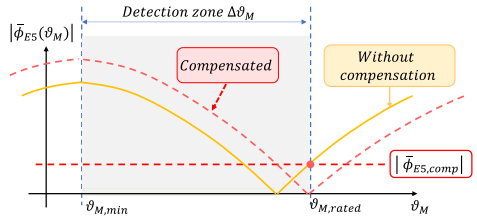

Fig. 8. Effect of the compensation angle.

The intervals where $\bar{f}_h^p$ has a monotonic trend are the same ones as $\bar{f}_h^r$.

D. Comparison between Radial and Parallel Magnetization

As the number of pole pairs increases, the differences between the mathematical models of the two types of magnetizations tend to decrease. Fig. 5 shows the ratio between the amplitude of the 5th harmonic component of the magnetic field in the air gap of radially and parallelly magnetized magnets for some values of the magnet arc. When the number of pole pairs exceeds three, the difference between the two magnetization models is less than 10%. If the number of pole pairs exceeds 4, the difference is less than 5%. Therefore, for motors with parallel magnetization and many poles, the permanent magnet magnetic field can be described with the radial magnetization model, which ensure accurate results with a simpler approach.

III. Fault Detection

In a six-phase PMSM, the current $\bar{\imath}_{S5}^S$ is not used for torque production and is typically zeroed to reduce the stator Joule losses and torque ripple [28]. To keep $\bar{\imath}_{S5}^S$ at zero, the control system must generate a voltage vector $\bar{v}_{S5}^S$ that compensates for the residual back-emf induced in the stator winding by the rotation of the rotor magnets. At steady state, the back-emf voltage can be written in terms of space vectors as follows:

$$\bar{v}_{S5}^S = \frac{d\bar{\varphi}_{E5}^S}{dt} = j\omega \sum_{h\in\{5\pm12n|n\in N\}}^{+\infty} h\,\bar{\phi}_{E,h}\, e^{jh\omega t} \tag{14}$$

$$\bar{\phi}_{E,h} = \frac{2\,\mu_0 N_S L\tau\; H_{R,M} K_{w,h}}{\pi^2 h^2}\,\bar{f}_h(\lambda_1,\lambda_2) \tag{15}$$

where L is the active length of the motor, τ is the pole pitch, $K_{w,h}$ is the stator winding factor, N_S is the number of conductors in series per phase, h is the harmonic order, and ω is the rotor speed in electrical radians.

The proposed model assumes that the back-emf induced by the rotor harmonic components of order higher than 10 is negligible. Under these conditions, $\bar{v}_{S5}$ can be written as follows:

$$\bar{v}_{S5}^S = \bar{v}_{S5,5}^S + \bar{v}_{S5,-7}^S \tag{16}$$

where:

$$\bar{v}_{S5,5}^S = j5\omega\,\bar{\phi}_{E,5} e^{j5\omega t} \tag{17}$$

$$\bar{v}_{S5,-7}^S = -j7\omega\,\bar{\phi}_{E,7} e^{-j7\omega t} \tag{18}$$

Equation (16) shows that $\bar{v}_{S5}^S$ is the sum of the 5th direct harmonic component and the 7th inverse harmonic component. The partial demagnetization of the rotor can be detected by analyzing the back-emf induced in the stator windings by the rotor. The demagnetization affects the phase and the magnitude of the harmonic components of the induced voltage. These effects are strongly dependent on the motor geometry and the parameters of the permanent magnets. In this paper, the variation in the magnitude of $\bar{v}_{S5}^S$ is used as fault index.

A. Control Scheme

The block diagram of the control system is shown in Fig. 6. In the control scheme, $\omega_{m,ref}$ is the speed command, and ϑ is the rotor position in electrical radians. The rotor speed is adjusted by Proportional Integral (PI) regulator (a), while the currents $i_{S1d,ref}$ and $i_{S1q,ref}$ are tracked by PI regulators (b) and (c). The current $i_{S1q,ref}$ is proportional to the motor torque, whereas $i_{S1d,ref}$ is set to zero to comply with the Maximum-Torque-Per-Ampere (MTPA) conditions.

To evaluate the back-emf of the motor, the current reference $i_{S5d,ref}$ and $i_{S5q,ref}$ are set to zero. To cancel the tracking error of $\bar{\imath}_{S5}$, PI regulators (d) and (e) are implemented in a reference frame rotating at 5ω, while PI regulators (f) and (g) are implemented in a d-q reference frame rotating at -7ω. The tuning of the current and speed regulators is based on the pole-zero cancellation by knowing the electrical parameters of the motor.

The voltage outputs of PI regulators (d)-(g) are constant quantities in steady-state conditions and provide the voltage space vectors $\bar{v}_{S5,5}$ and $\bar{v}_{S5,-7}$, that can be used as inputs of the diagnostic algorithm.

Finally, the PWM block calculates the gate signals of the six-phase inverter.

B. Diagnostic Algorithm

In three-phase PMSMs, the diagnosis of the state of health of the rotor magnets is typically based on the estimation of the back-emf induced on the stator windings [13]-[14]. These methods are usually simple but are affected by the torque level. In fact, (3) and (4) should be used to estimate the flux due to the rotor magnet $\bar{\varphi}_{E\rho}^S$. Therefore, the measurement of $\bar{\varphi}_{E1}^S$ depends on the parameters of the electric motor (stator resistance and inductance). Temperature variations and the magnetic saturation of the iron core can affect the accuracy of the measurement.

In multiphase machines, a new algorithm can be developed which preserves the simplicity of the previous method but makes the estimation of the fault more robust by exploiting the degrees of freedom available in multiphase drives.

In general, all the harmonic components of the $\bar{\varphi}_{E1}^S$ contain information related to the state of the rotor magnets, but the harmonic components of $\bar{v}_{S5}^S$ are not affected by the stator current $\bar{\imath}_{S5}^S$, which is set to zero by the control system [30]. Therefore, using $\bar{v}_{S5}^S$ allows one to estimate the corresponding flux $\bar{\varphi}_{E5}^S$ independently of the electrical parameters of the motor. If $\bar{\imath}_{S5}^S$ is zero, the machine in the vector subspace 5 behaves as it is in no-load conditions.

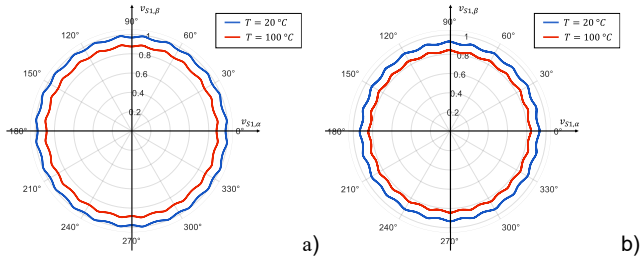

Fig. 9. Experimental waveforms of the back-emfs in subspace 1 at different temperatures in healthy conditions (a) and with trailing edge demagnetization (b).

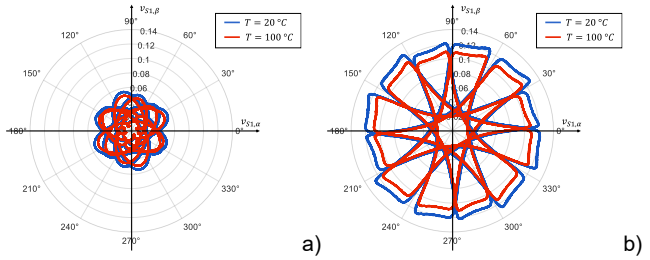

Fig. 10. Experimental waveforms of the back-emfs in subspace 5 at different temperatures in healthy conditions (a) and with trailing edge demagnetization (b).

In the six-phase SMPMSM used for the experimental validation in this paper, the magnitude of $\bar{v}_{S5,5}$ is higher than that of $\bar{v}_{S5,-7}$. Therefore, the fifth harmonic component has been selected as the input of the diagnostic algorithm to maximize the sensitivity and accuracy of the fault diagnosis.

The proposed algorithm can detect a rotor fault, estimate the demagnetization angle, and correct the alignment of the d-q reference frame. A schematic block diagram of the diagnostic algorithm is shown in Fig. 7.

The fifth harmonic component of the flux generated by the rotor magnet can be obtained from (17) as follows:

$$\bar{\phi}_{E,5} = -j\frac{\bar{v}_{S5,5}}{5\,\omega} \tag{19}$$

Under healthy conditions, the reference frame used for the control system is aligned with the fundamental harmonic of the $\bar{\phi}_{E,1}$, and $\bar{\phi}_{E,5}$ turns out to be a real-value quantity whose amplitude depends on the arc length ϑ_M of the magnet, as shown in Figs. 3 and 4.

During partial demagnetization, the symmetry axis of the magnets changes, and the control system loses the correct field orientation, so that the imaginary part of $\bar{\phi}_{E,5}$ becomes different from zero. This misalignment causes a decrease in the torque constant and local magnetic saturation of the iron core. Therefore, the proposed control algorithm aims to detect the demagnetization angle $\Delta\vartheta$ of the PMs and preserve the post-fault MTPA operation of the motor drive even under post-fault conditions.

As shown in Figs. 3 and 4, $\bar{\phi}_{E,5}$ is an injective function of ϑ_M only within predetermined intervals bounded by cusps. The compensation term $\bar{\phi}_{E5,comp}$ allows to maximize the convergence range of the diagnostic algorithm.

The effect of the compensation is shown in Fig. 8. For any value $\vartheta_{M,rated}$ of the magnet arc of the healthy motor, the compensation extends the injectivity region of $\bar{\phi}_{E,5}$ by moving the cusp to the boundary of the considered interval. In this way, the convergence region of the proposed algorithm for the fifth harmonic component is 72° electrical degrees.

After the compensation, the difference between the amplitudes of $\bar{\phi}_{E,5}$ and $\bar{\phi}_{E5,ref}$ is the input of a PI regulator, where $\bar{\phi}_{E5,ref}$ is the reference value of the magnetic flux predicted by the mathematical model of the magnet, which can be calculated by using (10), (12), and (15).

The PI regulator is saturated within the convergence region and finds the value of ϑ_M in steady state conditions that ensures the measured flux matches the one predicted by the mathematical model.

An apparent drawback of the developed algorithm is the limited extension of the detection zone (Fig. 8). Using the fifth harmonic, the maximum electrical demagnetization angle that can be detected is 72°. However, if necessary, the proposed scheme can be repeated in different convergence intervals to estimate even the complete rotor demagnetization ($\vartheta_M = 0$). It should be noted, however, that in the case of severe demagnetization faults, it may be sufficient to monitor the fundamental harmonic component.

Another important factor that can affect the effectiveness of the fault detection is temperature. A change in temperature alters the magnetic properties of the magnets with completely different consequences. The following section discusses these aspects in detail.

C. Temperature Effect

An increase in temperature reduces the remanence of the rotor magnets and may interfere with the detection algorithm based on back-emf estimation. The temperature distribution inside the magnets is generally not uniform for three-phase PMSM motors [30] - [32]. The higher harmonic orders of the stator magnetic field can induce eddy currents in the rotor resulting in uneven temperature distribution in the magnets. This phenomenon highly dependent on the waveform of the stator magnetic field distribution in the air gap and has dramatic impact on the performance of machines with concentrated stator windings. Eddy currents can be limited by segmenting and laminating the rotor magnets.

Compared to three-phase machines, multiphase machines have new degrees of freedom, which can be used to cancel out harmonic components other than the fundamental one. Therefore, the magnetic field distribution of the stator is close to a perfect sine. In order to evaluate this assumption, some thermal tests have been carried out on a couple of six-phase PMSMs, whose details are reported in Section IV. The results of this test are illustrated in Figs. 9 and 10, which show the loci of the back-emf when the motor is driven at constant speed at different magnet temperatures. The two motors have been heated by a long thermal test and then driven by an external motor for back-emf measurement. The distribution of the magnetic field at the air gap of the fundamental harmonic undergoes a uniform decrease both under the effect of temperature and local demagnetization (Fig. 9). Temperature uniformly modifies all the harmonic components, and this behavior is compatible with a uniform temperature distribution inside the magnets. Therefore, if the analysis is limited to the first harmonic component, it is difficult to distinguish the effect of temperature from that caused by irreversible demagnetization. On the other hand, if the analysis is extended to subspace 5, the scenario is completely different (Fig. 10). The *signature* of the fault caused by local demagnetization of the rotor magnets is completely different from that caused by a temperature increase. While temperature uniformly reduces the harmonic content of the

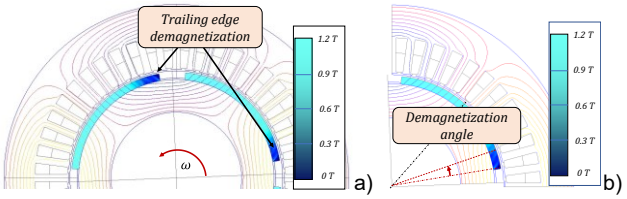

Fig. 11 Results of finite elements analysis. Magnet remanence after the demagnetization process (a) and demagnetization angle (b).

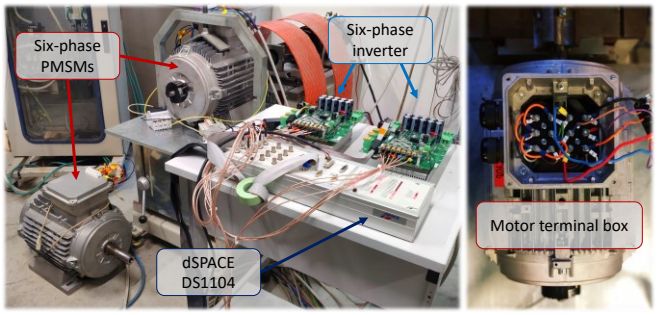

Fig. 12. Experimental setup.

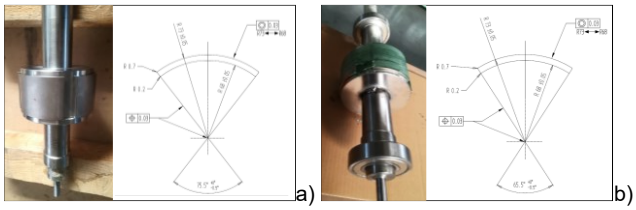

Fig. 13. Photos and design of the healthy (a) and the faulty (b) rotor magnets.

magnets, the local demagnetization varies the amplitude and the phase of all harmonics differently. As predicted by the theoretical analysis presented in this paper, some harmonic components may increase, and others may decrease.

The back-emf measurement is sufficient to diagnose the rotor demagnetization. However, the direct measurement of motor voltages is only sometimes possible. A no-load test should be performed with an external motor, and the outputs of six voltage probes should be acquired with a suitable acquisition system. The proposed method uses the same concept but can be applied online without external equipment.

In the control scheme of Fig. 6, the fifth and seventh harmonic components of the back-emf in subspace $\rho = 5$ are counterbalanced by the output of the harmonic PI regulators (d) – (g). Thus, the ratio $|\bar{v}_{5,5}|/|\bar{v}_{5,-7}|$ is not affected by a change in temperature. It changes due to a demagnetization fault, whose fundamental characteristic is to modify the amplitudes of the magnetic field harmonics, as shown in Figs. 3 and 4.

Furthermore, unlike a motor fault, the temperature does not misalign the reference frame $d_1 - q_1$ of the control system. As long as $\bar{\phi}_{E,5}$ is a real quantity and $\Delta\vartheta$ is zero, the rotor has not undergone a local demagnetization.

The following equation describes the relationship between the remanence and temperature T:

$$H_{Ci}(T) = H_{Ci}(T_0)[1 + \beta(T - T_0)] \qquad (20)$$

where T_0 is the reference temperature, β is the temperature coefficient, and $H_{Ci}(T_0)$ is the intrinsic coercivity at T_0. For magnetic materials, β is a negative number, so the performance of the permanent magnets decreases as the temperature increases. For NbFeB magnets, a typical value of this coefficient is $\beta = -0.007\ °K^{-1}$. This means that the back-emf induced by the rotor on the stator windings

TABLE I
PARAMETERS OF SIX-PHASE PMSMS

$R_S = 0.36\ \Omega$	$I_{s,rated} = 10\ A$	$p = 2$
$L_{S1} = 7.2\ mH$	$L_{S5} = 0.74\ mH$	$\omega_{rated} = 1000\ rpm$
$Moment\ of\ inertia\ J_M = 0.028\ Kg\ m^2$		
$Slot\ number = 48$		$Stator\ winding\ pitch = 15°$
$Magnetization\ type$ Parallel		$Magnet\ radial\ thickness$ 5 mm
$Healthy\ motor\ magnet\ arc$ 75.5°		$Faulty\ motor\ magnet\ arc$ 65.5°

TABLE II
MAGNETIC PROPERTIES OF NDFEBO

Properties	*Units*	*min*	*nominal*	*max*
Residual induction B_r	*mT*	*1130*	*1150*	*1170*
Coercivity H_{cB}	*kA/m*	*836*	*863*	*891*
Intrinsic coercivity H_{cJ}	*kA/m*	*1353*		
Curie temperature T_C	*°C*		*330*	

TABLE III
PARAMETERS OF THE DOUBLE THREE-PHASE INVERTER

$Infineon\ F12-25R12KT4G\ IGBT\ modules$	
$I_{max} = 25\ A_{peak}$	$E_{DC} = 300\ V$
$Switching\ frequency$ $f_{SW} = 10\ kHz$	$Dead\ time = 2\ \mu s$

decreases by 70% as the temperature increases by 100 °C. Partial demagnetization of the rotor magnets generally has a significant impact on the performance of the magnets. Therefore, a temperature variation may slightly reduce the accuracy of estimating the demagnetization angle but does not affect the fault detection, which is completely independent of thermal issues.

IV. EXPERIMENTAL RESULTS

A. Finite Elements Analysis Results

To evaluate the theoretical evidence and the assumptions of the paper, the behavior of the six-phase machine subjected to a demagnetization process has been simulated by finite element analysis using the Altair Flux software. The results of this analysis are shown in Fig. 11. Fig 11 (a) shows the effects of the trailing edge demagnetization due to load overcurrent six times the rated current and a temperature of 120 °C. This result shows that a current overload at high temperatures is sufficient to cause a local demagnetization of the magnets and to change the position of the north pole of the rotor magnetic field. The demagnetization takes place at the outer edge of the magnet, and the portion affected by the demagnetization depends on the magnetic field of the stator, which is generated by the overload current. The shape of the demagnetization edge depends on many motor design parameters, such as the number of slots, the slot opening length, the stator winding structure, and the rotor position at the time of the fault. Therefore, the demagnetization edge is not sharp as simplified in this paper, but an equivalent angle can be easily identified (Fig 11b). The primary objective of the diagnostic algorithm is not to accurately determine the demagnetized portion but rather to identify any issues with the rotor and find a comparable parameter to adjust the orientation of the reference frame used by the control system and restore the maximum torque capacity.

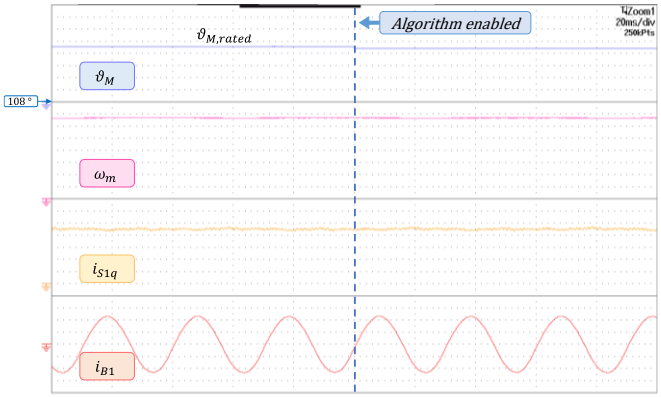

Fig. 14. Experimental results. Enabling transient of the diagnostic algorithm for the healthy motor at 10 Nm and 1000 rpm. Estimated Magnet arc ϑ_M (10°/div), rotor speed ω_m (150 rpm/div), i_{S1q} (2 A/div), and phase current i_{B1} (4 A/div).

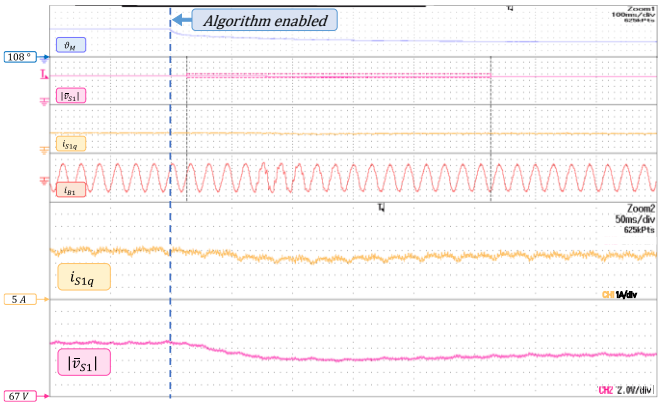

Fig. 16. Experimental results. Effect of realigning the reference frame after the fault detection at 10 Nm and 1000 rpm. Magnet arc ϑ_M (10°/div), $|\bar{v}_{S1}|$ (20 V/div – zoom 2 V/div), i_{S1q} (4 A/div – zoom 1 A/div), and phase current i_{B1} (4 A/div).

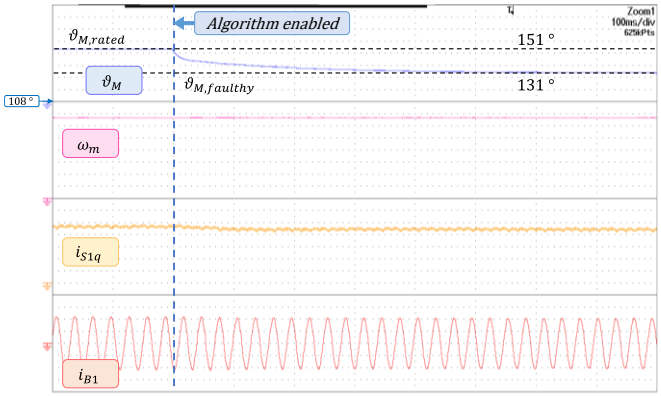

Fig. 15. Experimental results. Enabling transient of the diagnostic algorithm for the faulty motor at 10 Nm and 1000 rpm. Estimated magnet arc ϑ_M (10°/div), rotor speed ω_m (150 rpm/div), i_{S1q} (2 A/div), and phase current i_{B1} (4 A/div).

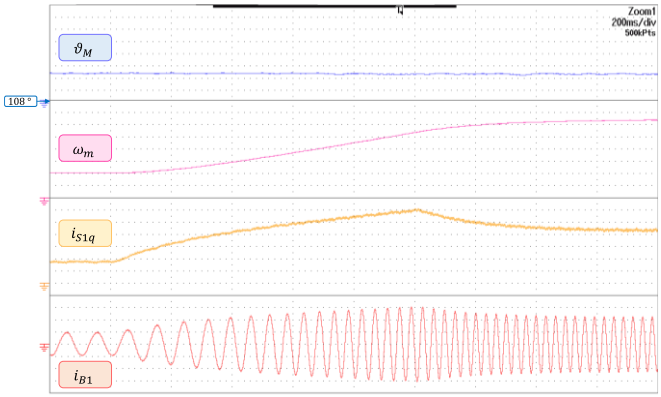

Fig. 17. Experimental results. Response of diagnostic algorithm during a torque and speed transient Estimated magnet arc ϑ_M (10°/div), rotor speed ω_m (150 rpm/div), i_{S1q} (1 A/div), and phase current i_{B1} (2 A/div).

B. Experimental setup

The effectiveness of the proposed diagnostic algorithm has been experimentally tested on two identical six-phase PMSMs, differing only in the extension of the magnet arc ϑ_M by 10 mechanical degrees (Figs. 12 and 13) .

The electrical and geometrical parameters of the two machines are listed in Table I, while Table II summarizes the main magnetic properties of rotor magnets.

One of the two motors has a reduced magnetic arc to emulate the partial demagnetization due to a current overload. For the faulty motor, the polar arc lengths of the rotor magnets have been reduced by 20° (electrical degrees) for all motor poles. For both motors, the rotor magnets are parallelly magnetized to experimentally evaluate the most complex situation.

The control schemes shown in Figs. 6 and 7 have been implemented using a rapid prototyping system based on dSPACE DS1104. The parameters of the power converter are summarized in Table III.

C. Experimental tests

Fig. 14 shows the behavior of the diagnostic algorithm for the healthy motor at the rated torque (10 Nm) and speed (1000 rpm) conditions. The diagnostic algorithm is initially disabled, and the initial value of the magnet arc is set to its nominal value $\vartheta_{M,rated}$. After enabling the fault diagnosis, the system estimates a value for the magnetic arc equal to the nominal value without any visible transient.

Fig. 15 shows the results of the same test carried out on the faulty motor under the same operating conditions. After a transient of about 500 ms, the diagnostic algorithm estimates a demagnetization angle of about 20 electrical degrees. The duration of the diagnostic transient depends on the bandwidth of the PI regulator in Fig. 7. The dynamic response of the diagnostic system must be calibrated to provide timely fault detection while avoiding unnecessary noise or overshoot responses.

Therefore, the algorithm can successfully detect the rotor demagnetization. In addition, the proposed solution can correct the alignment of the control system reference frame by modifying the actual angle ϑ. The main effect of this realignment is a slight reduction in the stator current i_{S1q} and the amplitude of the required voltage $|\bar{v}_{S1}|$ (Fig. 16). By means of the correction term $\Delta\vartheta$ calculated by the diagnostic algorithm of Fig. 7, the post-fault operation of the motor is still in MTPA conditions, which ensures the minimum stator Joule losses and the full exploitation of the DC-link voltage of the inverter.

It is worth noting that the stator copper losses depend quadratically on the phase current and even a slight reduction by 6% in i_{S1q}, as shown in Fig. 16, reduces the motor Joule losses by about 12%.

The torque waveform and the rotor speed are unchanged during the realignment.

In order to validate the robustness of the proposed solution, the response of the diagnostic algorithm during a speed and torque transient for the faulty machine is shown in Fig. 17.

Although the speed changes from 300 rpm to 1000 rpm and the presence of a torque transient as shown by i_{S1q}, the demagnetization angle remains almost unchanged. This experimental result proves that the proposed solution can detect demagnetization regardless of the operating conditions.

Obviously, below a certain speed threshold, it is no longer possible to detect demagnetization by (17). This speed was experimentally determined to be 150 rpm for the six-phase PMSM under test.

V. Conclusion

This paper proposes a mathematical model of the magnetic field in the airgap that can be adapted to different types of magnetizations. This model has been used to estimate the length of the rotor magnets and to evaluate the state of health of a six-phase PMSM.

The proposed algorithm can estimate the portion of the magnets lost during a demagnetization fault due to stator overcurrents.

The paper presents a complete control scheme that exploits the additional degrees of freedom of a six-phase PMSM. The diagnostic algorithm is based on the analysis of the back-emf waveform. In multiphase machines, unlike three-phase motors, it is possible to estimate some harmonic components of the voltage induced in the stator windings by setting the current space vector $\bar{\imath}_{S5}^{S}$ to zero. This makes it possible to extract information about the health state of the magnets independently of the electrical parameters of the motor.

Furthermore, the developed solution can correct the angular position of the field-oriented reference frame to maximize the torque capability and the efficiency of the motor even after the demagnetization fault.

The experimental results carried out on two six-phase SMPMSMs, which are structurally identical but differ in the size of the rotor magnets, were presented. They confirm that the demagnetization angle can be estimated independently of the motor operating conditions. The method is suitable for on-line monitoring of the permanent magnet health.

References

[1] B. Sarlioglu, C. T. Morris, D. Han and S. Li, "Driving Toward Accessibility: A Review of Technological Improvements for Electric Machines, Power Electronics, and Batteries for Electric and Hybrid Vehicles," *in IEEE Industry Applications Magazine*, vol. 23, no. 1, pp. 14-25, Jan.-Feb. 2017.

[2] R. Cao, C. Mi and M. Cheng, "Quantitative Comparison of Flux-Switching Permanent-Magnet Motors with Interior Permanent Magnet Motor for EV, HEV, and PHEV Applications," in *IEEE Transactions on Magnetics*, vol. 48, no. 8, pp. 2374-2384, Aug. 2012.

[3] J. O. Estima and A. J. Marques Cardoso, "Efficiency Analysis of Drive Train Topologies Applied to Electric/Hybrid Vehicles," in *IEEE Transactions on Vehicular Technology*, vol. 61, no. 3, pp. 1021-1031, March 2012.

[4] B. Sarlioglu and C. T. Morris, "More Electric Aircraft: Review, Challenges, and Opportunities for Commercial Transport Aircraft," in *IEEE Transactions on Transportation Electrification*, vol. 1, no. 1, pp. 54-64, June 2015.

[5] V. Madonna, P. Giangrande and M. Galea, "Electrical Power Generation in Aircraft: Review, Challenges, and Opportunities," in *IEEE Transactions on Transportation Electrification*, vol. 4, no. 3, pp. 646-659, Sept. 2018.

[6] W. Cao, B. C. Mecrow, G. J. Atkinson, J. W. Bennett and D. J. Atkinson, "Overview of Electric Motor Technologies Used for More Electric Aircraft (MEA)," in *IEEE Transactions on Industrial Electronics*, vol. 59, no. 9, pp. 3523-3531, Sept. 2012.

[7] A. Boglietti, A. Cavagnino, A. Tenconi, S. Vaschetto and P. di Torino, "The Safety Critical Electric Machines and Drives in the More Electric Aircraft: a Survey," 2009 35th *Annual Conference of IEEE Industrial Electronics*, 2009, pp. 2587-2594.

[8] B. Poudel, E. Amiri, P. Rastgoufard and B. Mirafzal, "Toward Less Rare-Earth Permanent Magnet in Electric Machines: A Review," in *IEEE Transactions on Magnetics*, vol. 57, no. 9, pp. 1-19, Sept. 2021.

[9] S. Morimoto, S. Ooi, Y. Inoue and M. Sanada, "Experimental Evaluation of a Rare-Earth-Free PMASynRM With Ferrite Magnets for Automotive Applications," in *IEEE Transactions on Industrial Electronics*, vol. 61, no. 10, pp. 5749-5756, Oct. 2014.

[10] K. Sone, M. Takemoto, S. Ogasawara, K. Takezaki and H. Akiyama, "A Ferrite PM In-Wheel Motor Without Rare Earth Materials for Electric City Commuters," in *IEEE Transactions on Magnetics*, vol. 48, no. 11, pp. 2961-2964, Nov. 2012.

[11] J. -H. Woo, T. -K. Bang, H. -K. Lee, K. -H. Kim, S. -H. Shin and J. -Y. Choi, "Electromagnetic Characteristic Analysis of High-Speed Motors with Rare-Earth and Ferrite Permanent Magnets Considering Current Harmonics," in *IEEE Transactions on Magnetics*, vol. 57, no. 2, pp. 1-5, Feb. 2021.

[12] J. Faiz and E. Mazaheri-Tehrani, "Demagnetization Modeling and Fault Diagnosing Techniques in Permanent Magnet Machines Under Stationary and Nonstationary Conditions: An Overview," in *IEEE Transactions on Industry Applications*, vol. 53, no. 3, pp. 2772-2785, May-June 2017.

[13] E. Mazaheri-Tehrani, J. Faiz, M. Zafarani and B. Akin, "A Fast Phase Variable abc Model of Brushless PM Motors Under Demagnetization Faults," in *IEEE Transactions on Industrial Electronics*, vol. 66, no. 7, pp. 5070-5080, July 2019.

[14] A. G. Espinosa, J. A. Rosero, J. Cusidó, L. Romeral and J. A. Ortega, "Fault Detection by Means of Hilbert–Huang Transform of the Stator Current in a PMSM With Demagnetization," in *IEEE Transactions on Energy Conversion*, vol. 25, no. 2, pp. 312-318, June 2010.

[15] H. Kao, W. -J. Wang, Y. -H. Lai and J. -W. Perng, "Analysis of Permanent Magnet Synchronous Motor Fault Diagnosis Based on Learning," in *IEEE Transactions on Instrumentation and Measurement*, vol. 68, no. 2, pp. 310-324, Feb. 2019.

[16] M. Skowron, T. Orlowska-Kowalska and C. T. Kowalski, "Detection of Permanent Magnet Damage of PMSM Drive Based on Direct Analysis of the Stator Phase Currents Using Convolutional Neural Network," *in IEEE Transactions on Industrial Electronics*, vol. 69, no. 12, pp. 13665-13675, Dec. 2022.

[17] F. Huang et al., "Demagnetization Fault Diagnosis of Permanent Magnet Synchronous Motors Using Magnetic Leakage Signals," in *IEEE Transactions on Industrial Informatics*, vol. 19, no. 4, pp. 6105-6116, April 2023.

[18] Y. Park et al., "Online Detection of Rotor Eccentricity and Demagnetization Faults in PMSMs Based on Hall-Effect Field Sensor Measurements," in *IEEE Transactions on Industry Applications*, vol. 55, no. 3, pp. 2499-2509, May-June 2019.

[19] Y. Park et al., "Online Detection and Classification of Rotor and Load Defects in PMSMs Based on Hall Sensor Measurements," in *IEEE Transactions on Industry Applications*, vol. 55, no. 4, pp. 3803-3812, July-Aug. 2019.

[20] D. Reigosa, D. Fernández, Y. Park, A. B. Diez, S. B. Lee and F. Briz, "Detection of Demagnetization in Permanent Magnet Synchronous Machines Using Hall-Effect Sensors," in *IEEE Transactions on Industry Applications*, vol. 54, no. 4, pp. 3338-3349, July-Aug. 2018.

[21] M. S. Rafaq et al., "Airgap Search Coil Based Identification of PM Synchronous Motor Defects," in *IEEE Transactions on Industrial Electronics*, vol. 69, no. 7, pp. 6551-6560, July 2022.

[22] H. Chen, C. Gao, J. Si, Y. Nie and Y. Hu, "A Novel Method for Diagnosing Demagnetization Fault in PMSM Using Toroidal-Yoke-Type Search Coil," in *IEEE Transactions on Instrumentation and Measurement*, vol. 71, pp. 1-12, 2022.

[23] V. Yaramasu, B. Wu, P. C. Sen, S. Kouro and M. Narimani, "High-Power Wind Energy Conversion Systems: State-Of-The-Art and Emerging Technologies," in *Proceedings of the IEEE*, vol. 103, no. 5, pp. 740-788, May 2015.

[24] F. Barrero and M. J. Duran, "Recent Advances in the Design, Modeling, and Control of Multiphase Machines—Part I," in *IEEE Transactions on Industrial Electronics*, vol. 63, no. 1, pp. 449-458, Jan. 2016.

[25] M. J. Duran and F. Barrero, "Recent Advances in the Design, Modeling, and Control of Multiphase Machines—Part II," in IEEE Transactions on Industrial Electronics, vol. 63, no. 1, pp. 459-468, Jan. 2016.

[26] A. Tani; Y. Gritli; M. Mengoni; L. Zarri; G. Sala; A. Bellini and G. Serra, "Detection of Magnet Demagnetization and High-Resistance Connections in Five-Phase Surface-Mounted Permanent Magnet Generators," 2015 IEEE *10th International Symposium on Diagnostics for Electrical Machines, Power Electronics and Drives (SDEMPED),* 2015, pp. 487-493.

[27] M. Mengoni, L. Vancini, A. Tani, Y. Gritli, L. Zarri and C. Rossi, "On-line Detection of Magnet Demagnetization in Asymmetrical Six-Phase

Surface-Mounted Permanent Magnet Synchronous Motor Drives," 2019 *IEEE 12th International Symposium on Diagnostics for Electrical Machines, Power Electronics and Drives (SDEMPED)*, 2019, pp. 188-194.
[28] Y. Hu, Z. Zhu and K. Liu, "Current Control for Dual Three-Phase Permanent Magnet Synchronous Motors Accounting for Current Unbalance and Harmonics," in *IEEE Journal of Emerging and Selected Topics in Power Electronics*, vol. 2, no. 2, pp. 272-284, June 201.
[29] F. Dubas and C. Espanet, "Analytical Solution of the Magnetic Field in Permanent-Magnet Motors Taking into Account Slotting Effect: No-Load Vector Potential and Flux Density Calculation," in *IEEE Transactions on Magnetics*, vol. 45, no. 5, pp. 2097-2109, May 2009.
[30] J. Malvar et al., "Graphical Diagram for Subspace and Sequence Identification of Time Harmonics in Symmetrical Multiphase Machines," in IEEE Transactions on Industrial Electronics, vol. 61, no. 1, pp. 29-42, Jan. 2014.
[31] D. D. Reigosa, D. Fernandez, T. Tanimoto, T. Kato and F. Briz, "Permanent-Magnet Temperature Distribution Estimation in Permanent-Magnet Synchronous Machines Using Back Electromotive Force Harmonics," in IEEE Transactions on Industry Applications, vol. 52, no. 4, pp. 3093-3103, July-Aug. 2016.
[32] D. Liang et al., "Estimation of Two- and Three-Dimensional Spatial Magnet Temperature Distributions for Interior PMSMs Based on Hybrid Analytical and Lumped-Parameter Thermal Model," in IEEE Transactions on Energy Conversion, vol. 37, no. 3, pp. 2175-2189, Sept. 2022.

Luca Vancini received the M.Sc. and Ph.D. degrees in Electrical Engineering from the University of Bologna, Bologna, Italy, in 2018 and 2022, respectively. Currently, he is a Research Fellow with the Department of Electrical, Electronic and Information Engineering “G. Marconi,” University of Bologna. His research interests include power electronics, control of multiphase converters, and diagnostic techniques for multiphase machines.

Michele Mengoni received the M.Sc. (with honors) and Ph.D. degrees in electrical engineering from the University of Bologna, Bologna, Italy, in 2006 and 2010, respectively. He is currently an Associate Professor with the Department of Electrical, Electronic and Information Engineering "G. Marconi," University of Bologna. His research interests include the design, analysis, and control of three phase electric machines, multiphase drives, and ac/ac matrix converters. Currently, he serves as an Associate Editor for IEEE Trans. on Industrial Electronics.

Gabriele Rizzoli received the M.Sc and Ph.D. degrees in Electrical Engineering, with honors, respectively in 2012 and 2016, from the University of Bologna, Bologna, Italy. He is currently an Assistant Professor with the Department of Electrical, Electronic and Information Engineering “G. Marconi” of the University of Bologna.
His research interests include the design of electrical machines, the development and control of high-efficient power converters for automotive and renewable energy applications.

Luca Zarri received the M. Sc. and Ph.D. degrees in Electrical Engineering from the University of Bologna, Bologna, Italy, in 1998 and 2007, respectively. Currently, he is a Full Professor of power electronics, electrical machines and drives with the Department of Electrical, Electronic, and Information Engineering “Guglielmo Marconi”, University of Bologna. He has authored or coauthored more than 170 scientific papers. His research activity concerns the control of power converters and electric drives. He is a senior member of the IEEE Industry Applications, IEEE Power Electronics and IEEE Industrial Electronics Societies. Currently, he is the Chair of the IEEE IAS Industrial Drives Committee.

Angelo Tani received the M. Sc. degree in Electrical Engineering, with honors, from the University of Bologna, Bologna, Italy, in 1988. Currently he is a Full Professor of power electronics, electrical machines and drives with the Department of Electrical, Electronic and Information Engineering “Guglielmo Marconi”, University of Bologna. He has authored more than 200 papers published in technical journals and conference proceedings. His current activities include modelling, control and fault diagnosis of multiphase electric machines.